The effect of CoPt crystallinity and grain texturing on properties of exchange-coupled Fe/CoPt systems

H. Oguchi,[1,a)] A. Zambano,[1] M. Yu,[1,2] J. Hattrick-Simpers,[1,5] D. Banerjee,[1] Y. Liu,[3] Z. L. Wang,[3] J. P. Liu,[4] S. E. Lofland,[5] D. Josell,[6] and I. Takeuchi[1]
[1]*Department of Materials Science and Engineering, University of Maryland, College Park, Maryland 20742, USA*
[2]*Advanced Materials Research Institute, University of New Orleans, Louisiana 70148, USA*
[3]*School of Materials Science and Engineering, Georgia Institute of Technology, Atlanta, Georgia 30332, USA*
[4]*Department of Physics, University of Texas at Arlington, Arlington, Texas 76019, USA*
[5]*Department of Physics and Astronomy, Rowan University, Glassboro, New Jersey 08028, USA*
[6]*Metallurgy Division, National Institute of Standards and Technology, Gaithersburg 20899, Maryland, USA*

(Received 5 June 2008; accepted 8 December 2008; published online 23 January 2009)

The effect of the crystallinity and the grain texturing of CoPt hard layers on exchange coupled Fe/CoPt soft/hard magnetic systems was studied using gradient thickness multilayer thin films. We have studied the hard layer structures by transmission electron microscopy and x-ray diffraction, and characterized the exchange coupling interaction through magnetization loops obtained by the magneto-optical Kerr effect measurement. We found that exchange coupling strongly depends on the crystalline characteristics of the CoPt hard layer. There is correlation between the mixture of different grain orientations of the CoPt hard layer and coupling efficiency. In particular, interlayer coupling is enhanced when there is only one orientation, namely, the $L1_0$ CoPt structure with its *c*-axis inclined at 45° with respect to the substrate plane. An increased degree of mixture of the latter with the in-plane-*c*-axis $L1_0$ CoPt structure is detrimental to obtaining one-phase-like magnetization loops. The present work points to the importance of controlling the crystalline properties of the hard layer in order to enhance the maximum energy product $(BH)_{max}$ in hard/soft nanocomposite magnets. © *2009 American Institute of Physics*. [DOI: 10.1063/1.3068330]

Magnetic thin film multilayers are ubiquitous in a variety of device structures such as magnetic tunnel junctions and magnetic recording media, and exchange coupling between layers critically determines the overall behavior of the devices. Previously, soft/hard magnetic bilayers have also been used as a simple one-dimensional model for studying the properties of exchange-coupled nanocomposite magnets.[1,2]

Exchange coupling between the hard magnetic phase and the soft magnetic phase is the key to enhance maximum energy product ($(BH)_{max}$) (Refs. 2–14) of such magnets. However, currently reported experimental $(BH)_{max}$ values of exchange-coupled bulk magnets are far below the theoretically predicted ones. This suggests that the coupling behavior between the hard and the soft magnet needs to be improved. In order to achieve better coupling, the effects of various factors such as interface conditions,[15,16] soft-hard volume fraction,[17] microstructures,[18–23] etc., have been investigated. There have been some theoretical and empirical works carried out to elucidate how these factors can alter the coupling mechanism.[24–28] However, there has been limited work on the effect of grain texturing.[29]

In this report, we investigate the effects of the hard layer crystallinity and grain texturing on the exchange coupling between hard/soft magnetic bilayers. The thin film bilayers are useful for systematically studying the effect of precisely controlled thicknesses, and the epitaxial growth allows for the investigation of the role of crystal orientation and structure as previously reported.[5,7,30,31] We used the high-throughput gradient approach,[32,33] where a large number of samples with continuously changing thicknesses are fabricated and measured simultaneously. This allows us to rapidly and systematically investigate the effect of one parameter at a time. To study the hard layer crystallinity and grain-texturing effects, we fixed the other parameters such as the interface roughness, the hard layer thickness, and the degree of interdiffusion between the layers. This method provides systematic information necessary to delineate the subtle variation in the behavior of exchange coupling as a function of the hard layer crystallinity and grain texturing. Fe was used as the soft layer which has a large saturation magnetization and low H_c, and CoPt was used as the hard layer which has a high H_c and low saturation magnetization. Fe/CoPt soft/hard magnetic bilyer thin films were deposited in a high-vacuum combinatorial electron-beam (e-beam) deposition chamber (with the base pressure $\approx 3\times10^{-8}$ Torr). The chamber has two e-beam guns with two movable copper crucibles, each of which contains six pockets for metal targets, and two computer-controlled movable shadow masks. This allows us to deposit up to 36 different combinations of metallic layers without breaking the vacuum on 1.5×1.5 cm^2 substrate. By synchronizing the motion of the shadow masks with the evaporation rates of the targets, we can fabricate thin films in precisely controlled areas, with controlled compositions, and gradient thickness in two perpendicular direc-

a)Electronic mail: ohguchi@mail.umd.edu.

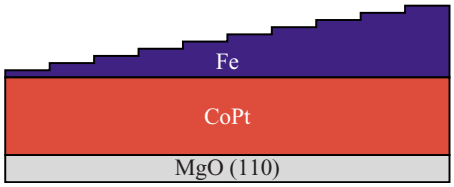

FIG. 1. (Color online) Schematic of the typical sample design.

tions. The advantage of this technique is that we can grow multiple samples on an individual chip under the same set of conditions, which reduce subtle run-to-run variations in the conditions, and we can perform systematic and high-throughput studies. In this experiment, simple bilayer samples with gradient thickness in one direction were fabricated.

Figure 1 shows the cross-sectional schematic of a typical design of the Fe/CoPt soft/hard bilayer gradient sample. The top Fe layer has a stepwise gradient thickness. In this work, we studied three gradient samples, A, B, and C, whose difference is in their CoPt crystallinity. CoPt films were grown epitaxially on MgO (110) substrates, after deposition of a 1-nm-thick Pt buffer layer at 500 °C (not shown). Then a 30-nm-thick CoPt hard layer was deposited at 450 °C on sample A and at 500 °C on samples B and C. Sample C was then annealed at 500 °C for 15 min in vacuum, while sample B was not. All three samples were cooled down to room temperature before the deposition of the Fe soft layer. The Fe soft layer was deposited with a stepwise thickness gradient from 0 to approximately 10 nm over 10 mm, which is the length of each sample chip. To prevent oxidization, the gradient samples were capped with a 5–8-nm-thick Au layer (not shown). The stepwise Fe thickness (t_{Fe}) gradient allows us to systematically determine the critical Fe thickness to obtain an ideal hard-soft layer exchange coupling. Previously, we have used this technique to delineate the dependence of the exchange length on the soft magnetic parameters.[28]

Crystallinity and the out-of-plane orientation of the epitaxially grown CoPt hard layers were studied by a Bruker D8 x-ray diffractometer (XRD) with an area detector using Cu $K\alpha$ radiation (0.154 18 nm). The pole figure measurements were performed to establish the relative epitaxial relations between the CoPt layer and the MgO substrate. The microstructure of the CoPt hard layer was studied using transmission electron microscopy (TEM). Magnetic hysteresis (M-H) loops were obtained using the magneto-optical Kerr effect (MOKE) measurement. Our MOKE set up uses a 635 nm laser (Blue Sky Research, CLAS-635–025-WL00), whose beam diameter is focused down to less than 0.5 mm, which is smaller than the step width of the Fe thickness gradient, and fixed throughout a set of measurement. The relatively small beam spot together with a movable sample stage allows us to measure many spots with different Fe thicknesses across each gradient sample in a relatively short period of time. (This sentence here is OK.) The magnet for the MOKE set up can apply up to 2 T, which is large enough to magnetically saturate our CoPt hard layers. It is important to note that MOKE is a surface sensitive measurement, and

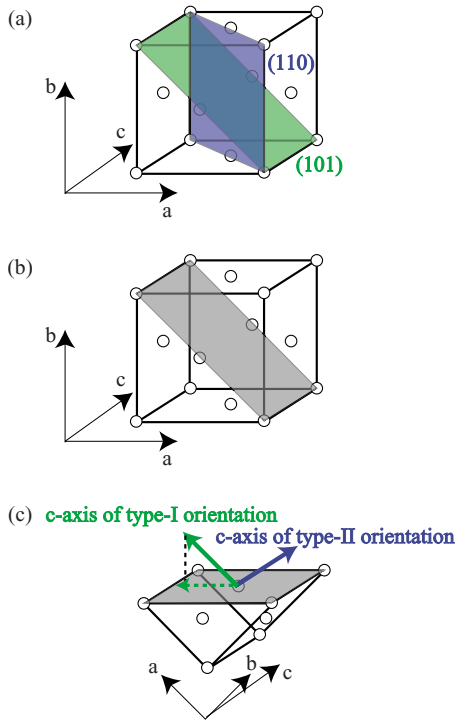

FIG. 2. (Color online) Typical crystal structures of (a) fcc MgO and (b) fct CoPt. (c) The MgO (110) plane is rotated 45° along c-axis of MgO. Green and blue arrows are easy axis (c-axis) of type-I orientation and type-II orientation.

the penetration depth of the laser for the samples studied here was empirically determined to be about 10 nm.

Given the lattice match between the MgO substrate and the CoPt hard layer, two different types of CoPt $L1_0$ structure orientations can be epitaxially grown on MgO(110): one with its c-axis inclined at ≈45° with respect to the substrate plane (type-I orientation) and another with its c-axis in the substrate plane (type-II orientation).[34,35] Figures 2(a) and 2(b) show the typical crystal structures of fcc MgO and fct CoPt, respectively. In Fig. 2(c), the MgO (110) plane is rotated 45° along the c-axis of the MgO substrate so as to facilitate the visualization of the film growth configuration in the MgO [110] direction. This also helps to visualize, in the actual system, the magnetic easy axis (c-axis) of type-I orientation, whose in-substrate-plane projection is parallel to MgO $[1\bar{1}0]$ and that of type-II orientation, which is parallel to MgO [001].

Figure 3 shows the θ-2θ XRD patterns of the CoPt hard layer in the three samples. Patterns of samples A–C are indicated by colors red, blue, and green, respectively. At around 33.3°, samples B and C show the CoPt (110) peak with a higher intensity than the same peak in sample A. The CoPt (110) peak comes from type-II orientation only. This clearly shows the difference in the CoPt structure in each sample, indicating that samples B and C have a larger amount of type-II grains than sample A does. At around 71°, a high-intensity broad peak is observed for all three samples. This is the overlapping of the CoPt (220) peak, which is associated with grains with type-II orientation, and the CoPt (202) peak, which is associated with grains with type-I orientation. The inset shows the peak at around 71° more

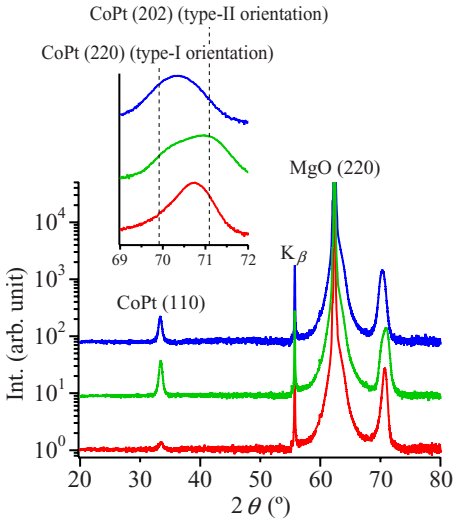

FIG. 3. (Color online) XRD patterns of samples A (red), B (green), and C (blue). Inset: magnification of the mixed peak region.

clearly. The change in the peak shape and their peak position shift is attributed to changes in the structure and the relative volume fraction in the mixture of grains with the two orientations.

A pole figure XRD analysis was performed to investigate the in-plane epitaxial relationship between the MgO substrate and the CoPt thin film (Fig 4). The CoPt (201) planes of type-I orientation and type-II orientaitions, and the MgO (200) plane were observed at χ angles of 16.3°, 49.8°, and 43.5°, respectively. A twofold symmetry is seen for MgO (200) (gray spots) at the same φ angles for CoPt (201) of type-I orientation (green spots). CoPt (201) of type-II orientation (blue spots) appears symmetrically on either side of the MgO (200) peaks. The φ angle between type-I and type-II of CoPt (201) planes is ≈36.7° as measured from the pole figure. This value agrees well with the expected interplanar angle of 36.0°, which can be estimated using the literature values of the lattice parameters, namely, a =0.380 300 nm and c=0.370 100 nm.[36] Because type-I and type-II reflections are observed as well-defined peaks rather than a ring at the expected φ angle, an epitaxial relationship between the MgO (110) substrate and the CoPt thin film is confirmed.

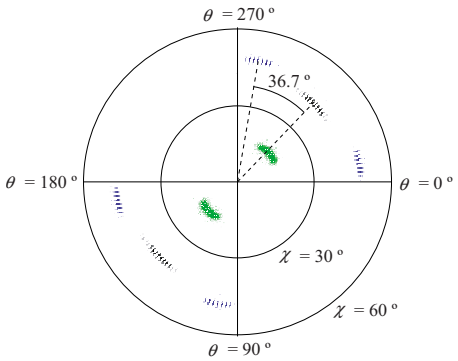

FIG. 4. (Color online) Pole figure of the CoPt (201) of type-I orientation (green) and type-II orientation (blue) on the MgO (110) substrate, together with the MgO (200) (gray).

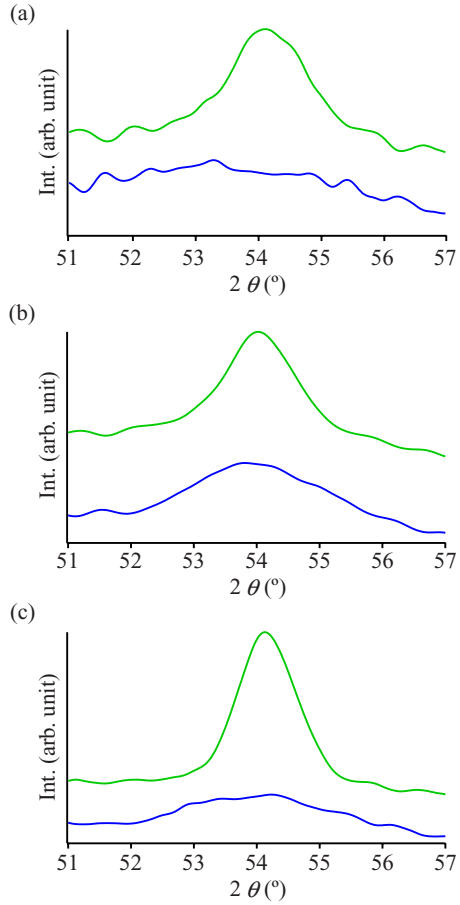

FIG. 5. (Color online) θ-2θ XRD patterns of the CoPt (201) peaks of type-I orientation and type-II orientation of each sample.

To estimate the volume fraction of each type of orientation, we looked at θ-2θ XRD scans. The idea is to find a set of planes that allows us to see peaks coming from the two types of grain orientations separately: the same indexed peak would appear separately in the reciprocal space coming from different grain orientations. As shown in Fig. 5, for each sample, we have used the CoPt (201) peaks for the two grain orientations. The volume fraction V for each orientation, I or II, was calculated as

$$V_{I,II} = \frac{\text{peak area}_{I,II}}{(\text{peak area}_I) + (\text{peak area}_{II})}.$$

Here, peak area is the integrated peak area in the spectrum. The peak intensity of the CoPt (201) coming from type-II orientation is very weak for sample A It is slightly stronger for sample B, and well pronounced for sample C [see Figs. 5(a)–5(c) for samples A–C, respectively]. This results in a decrease in V_I and an increase of V_{II} as seen in Table I. This indicates that the CoPt hard layer goes from mostly consist-

TABLE I. Volume fraction of type-I orientation grains (V_I) and type-II orientation grains (V_{II}) in each sample.

	Sample A	Sample B	Sample C
V_I	≈1	0.84	0.54
V_{II}	≈0	0.16	0.45

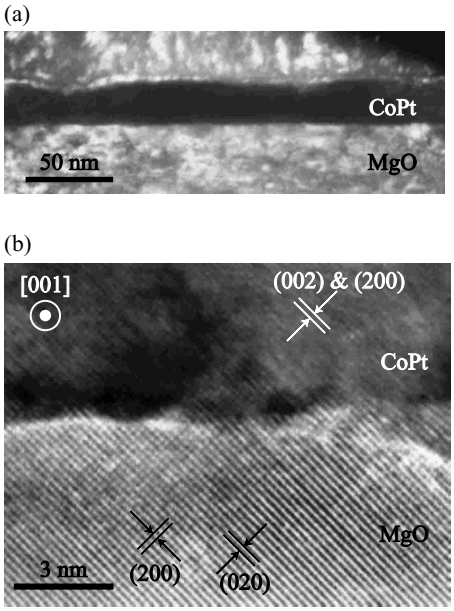

FIG. 6. (a) A cross-sectional dark field image and (b) cross-sectional high-resolution image of sample B.

ing of type-I grains in sample A to being a more balanced mixture in sample C.

Figure 6 shows typical TEM cross-sectional images taken along [001] of the MgO substrate. The images are from sample B, but the main features seen in the images are representative of all three samples. The dark field image in Fig. 6(a) shows a Fe/CoPt system with a low interface roughness. This reduces uncertainties coming from the orange peel effect[18] and simplifies the one-dimensional analysis. In Fig. 6(b), a high-resolution image shows the MgO (200) and MgO (020) lattice planes, as well as the CoPt (002) and/or the CoPt (200) lattice plane of type-I and/or type-II grains, respectively. The spacing of the CoPt (002) planes in type-I grains and the CoPt (200) planes in type-II grains are 0.1848 and 0.1908 nm, respectively. This similarity in value makes it difficult to distinguish the orientations by simply studying the images. There is a clear MgO/CoPt interface, and there is no sign of discontinuity of the lattice planes. This confirms the epitaxial growth of the CoPt hard layer.

From dark field images and high-resolution images of several Fe/CoPt systems including Figs. 6(a) and 6(b), we conclude the typical root mean square surface roughness is less than 1 nm, which is small enough compared with our laser penetration depth of MOKE. Therefore, the effect of the interface roughness on the *M-H* hysteresis loops obtained using MOKE (discussed later) should be negligible.

The two CoPt grain orientations have different magnetic easy axes relative to the substrate, whose combination leads to the effective easy axis of each sample. Our CoPt hard layers have larger fractions of type-I orientation grain than type-II orientation grain fraction (see Table I). To empirically determine the effective easy axis, we measured the *M-H* loops for external field applied along two MgO directions: $[1\bar{1}0]$ and [001] (see Fig. 7). Type-I orientation has a substrate in-plane projection parallel to MgO $[1\bar{1}0]$, and that of type-II orientation is parallel to MgO [001]. The *M-H* loop

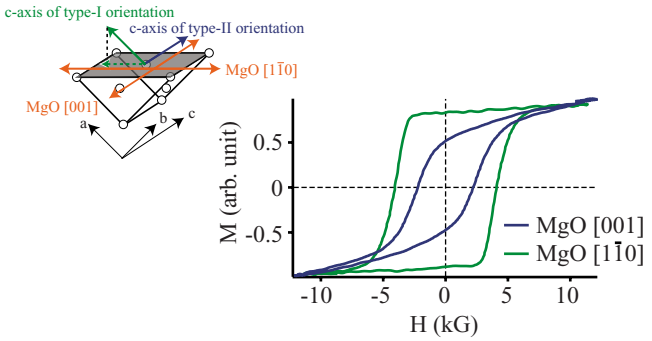

FIG. 7. (Color online) Normalized *M-H* hysteresis loops measured with applied field along the MgO [001] (blue) and the MgO $[1\bar{1}0]$ (green). Inset: easy axis of type-I orientation grains (green) and type-II orientation grains (blue).

obtained with the applied external field along the [001] direction has a smaller H_c and increasing magnetization even after the loop is closed, indicating that this direction is the hard axis. On the other hand, the *M-H* loop obtained with the applied external field along the $[1\bar{1}0]$ direction has a larger H_c and saturated magnetization when the loop is closed, indicating that this direction is the easy axis. All *M-H* loops shown in the rest of this were obtained by applying the magnetic field along the $[1\bar{1}0]$ direction of the MgO substrate.

An ideally exchange-coupled hard/soft magnetic systems shows a one-phase-like square *M-H* loop. We use this as a qualitative measure of good coupling interaction. In contrast, a nonideal exchange-coupled magnet exhibits a nonsquare one-phase-like or two-phase-like *M-H* loop with a step and/or deflection in the shape of the loop. We use occurrence of such features as indication of nonideal coupling interaction (even if the system has a high coercive field). This could be due to nonuniform coupling interaction, where the local coupling behavior might depend on the structure of the hard layer.

In order to study the exchange coupling of many spots on each sample, where each spot has a different Fe thickness (t_{Fe}), we took an *M-H* loop at each spot on each sample using MOKE and plotted them together in Figs. 8(a)–8(c) for samples A–C, respectively. [(a)–(c) need to come first, please rearrange the figure.]

To confirm that the exchange coupling behavior we are deducing with MOKE from each individual spot area provides an accurate description of the magnetic properties of the interface region of the local soft/hard bilayer, we have compared the MOKE *M-H* loops with *M-H* loops taken using a vibrating sample magnetometer (VSM). In particular, we cut sample A into two pieces and measured the piece where the t_{Fe} is more than 10 nm. The *M-H* loops taken using the VSM and the MOKE are normalized and plotted together in Fig. 8(d). The coercive field of two *M-H* loops appears at $H \approx 3$ kG in both curves (this does not look like 3 kG to me, do you mean more like ~2 kG? are you talking about the "nucleation,"? I thought we always called this nucleation?), and the general shapes of the curves are in good agreement with each other. The difference in two *M-H* loops occurs as a deflection at a higher field seen in the VSM

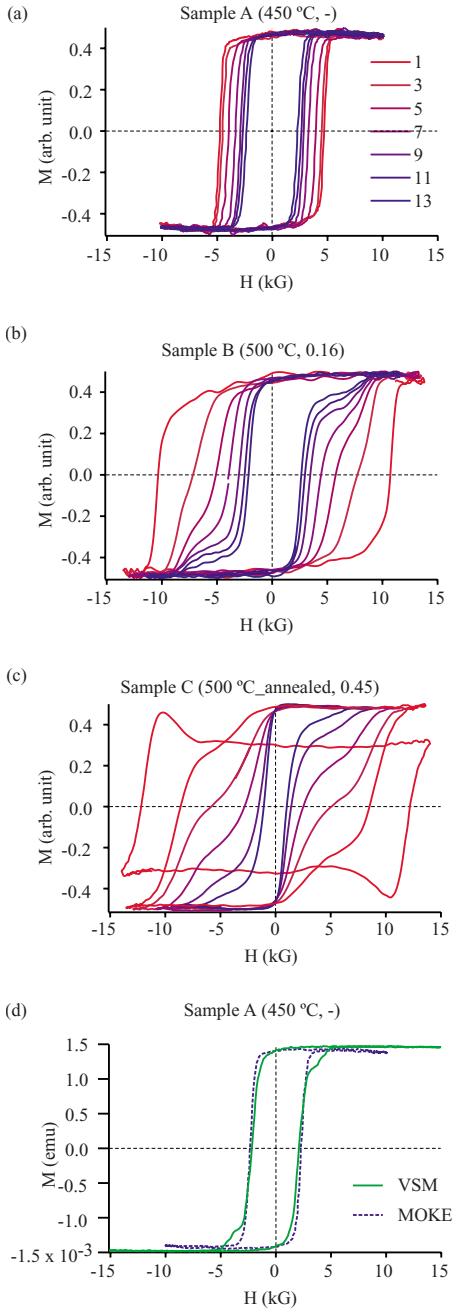

FIG. 8. (Color online) Normalized *M-H* hysteresis loops of various Fe soft layer thicknesses t_{Fe} on the CoPt hard layer. The thickness of the Fe soft layer t_{Fe} (nm) is indicated by color legend added on (a). In parenthesis: growth condition of the CoPt hard layer and volume fraction of type-II orientation grains. (d) *M-H* hysteresis loops of sample A obtained using MOKE (dashed black) and VSM (solid green) are plotted together for comparison.

curve. The relevant difference between the MOKE measurement and the VSM measurement is the measurement depth. Namely, the entire thickness of the sample is measured by VSM, but only the surface region is probed by MOKE. Therefore, the difference between two *M-H* loops is indicating a presence of a weekly coupled or decoupled CoPt hard layer in the region deeper than the penetration depth of the laser (≈10 nm) used in this study. Since the thickness of the hard layer (30 nm) used in this study is more than the typical domain wall width of the CoPt hard magnet, it is reasonable to have different magnetic behaviors in a single CoPt hard layer.

(Is this like a two-phase behavior inside CoPt? Then we should say this—and also, is this really true that our CoPt individual film is not single phase like?) Thus, the surface sensitivity of MOKE allows us to selectively study the bilayer interface region where the exchange coupling takes place.

To study the exchange coupling behavior in each sample, *M-H* loops of samples with different Fe thickness t_{Fe} were obtained and plotted together in Figs. 8(a)–8(c) for samples A–C, respectively. Because the penetration depth of the laser beam used in our MOKE system is ≈10 nm, in general, the thinner t_{Fe} is, the weaker the magnetic contribution of the Fe soft layer to the shape of the *M-H* loops is. For very thin layer of Fe $t_{Fe} \approx 1$ nm, most of the signal in the MOKE measurement comes from the hard layer. The *M-H* loops from the thinnest Fe layer ($t_{Fe} \approx 1$ nm) region gives information about magnetic behavior of the CoPt hard layer. Figure 8 shows variation of the coercive field of the CoPt hard layer of each sample. The coercive field of the CoPt layer is 5, 11, and 13 kG for samples A, B, and C, respectively. This increase in the coercive field of the CoPt layer is directly correlated with increase in V_{II} and increase in the mixture of two types of orientations (Table I). The increase in V_{II} and the mixture of the two orientations also enhances the two-phase-like behavior of the CoPt layer (see Fig. 8). Namely, an extra small first step seen in the magnetization curves during magnetic reversal gets more pronounced as the grain orientation mixture increases. As seen in Fig. 8, Sample A shows a one-phase-like CoPt *M-H* loop behavior, but sample C shows a clear two-phase-like CoPt *M-H* loop behavior.

As t_{Fe} increases, all three samples show decrease in their coercive field attributed to the softening of the CoPt hard layer. To further understand the magnetic behavior of the entire system, we define two quantities. H_{c_small}, which is the smaller applied external field at which first maximum slope of the *M-H* loops appears, and H_{c_large}, which is the largest applied external field at which second maximum slope of the *M-H* loops appears (see Fig. 8). Because of the increasing degree of demagnetization as a function of increasing t_{Fe}, it is evident that the first demagnetization region of the two-phase-like *M-H* loops corresponds to the Fe contribution to the total magnetization and that H_{c_small} represents the coercive field of the Fe soft layer. Thus, monitoring the position of the H_{c_small} provides a means to characterize the behavior of the soft layer. H_{c_large} is associated with the behavior of the CoPt hard phase.

Figure 9 shows H_{c_small} and H_{c_large} versus t_{Fe} for each sample. In general, H_{c_large} decreases with increasing t_{Fe} due to the softening of the CoPt hard layer. This variation is more pronounced in samples B and C, whose CoPt hard layers are mixture of grains with the two types of orientations. Sample A has $H_{c\_small}=H_{c\_large}$, which is a sign of strong coupling interaction. This sample has only one grain orientation. As already mentioned, an increase in the mixture of the two CoPt orientations is also correlated with the appearance of the two-phase-like behavior in samples B and C. In sample B, despite showing a decrease in H_{c_small} with increasing t_{Fe},

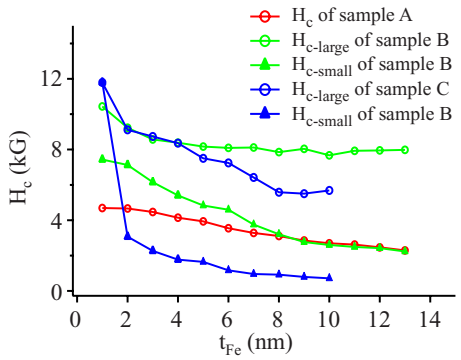

FIG. 9. (Color online) Coercive field of the first and second demagnetization of the magnetization loops (Fig. 8) as a function of thickness of the Fe soft layer t_{Fe}. Samples A (red), B (green), and C (blue).

H_{c_small} values are high and change considerably as t_{Fe} increases. These are signs of a relatively weak coupling. For sample C, H_{c_small} do not decrease with increasing t_{Fe}. The Fe layer seems to have a nonuniform interaction and follows the behavior of the part of the CoPt layer associated with the first demagnetization only. In addition, H_{c_small} values are the lowest. These observations indicate that sample C has the weakest coupling among the three samples. It is clear that the overall exchange coupling behavior of a system strongly depends on the CoPt structure, and in particular, on the degree of mixture of its grain orientations.

Suzuki *et al.*[37,38] previously reported that the exchange constant A_{int}, which is the measure of the strength of the exchange coupling, strongly depends on the crystallinity of the magnetic bilayer system. In their report, they discussed A_{int} of the single-crystalline sample with no grain mixture and the polycrystalline sample with significant grain mixturing. They observed a two order of magnitude smaller A_{int} for the polycrystalline bilayer system compared to that for the single-crystalline bilayer system. This decrease in A_{int} can be the reason why the exchange coupling of our soft/hard bilayer systems becomes weaker with a higher degree of mixture of grain orientations.

In summary, Fe/CoPt soft/hard magnetic bilayers were grown on MgO (110) substrates. Epitaxial growth of CoPt hard layers studied in this work consisted of two directional $L1_0$ orientations; type-I (101), with its easy axis along MgO [100] and type-II (110), with its easy axis along MgO [001]. The volume fraction of each grain orientation was varied by changing the deposition temperature and the heat treatment of the hard layer. An increase in the squareness of the CoPt hard layer magnetic loop is observed when only type-I orientation grains are present. The presence of the single phase grain orientation resulted in the best coupling between the CoPt hard layer and the Fe soft layer giving rise to the one-phase-like magnetization loops. When the fraction of type-II orientation grain (or equivalently the mixture of grain orientations) is increased, magnetization loops of the CoPt hard layer exhibit a two-phase-like behavior. The latter is accentuated when the Fe layer is present, indicating that interlayer coupling is nonuniform. The coupling behavior might depend on the local coercive field of the hard layer. Thus, suppressing the mixture of the two types of grain orientations is beneficial to the enhancement of ideal exchange coupling interaction. In order to increase the maximum energy product $(BH)_{max}$, it is crucial to have one-phase-like magnetic loops with high coercive fields. Therefore, one should not only focus on increasing the coercive field of the hard phase but also on monitoring the squareness of its magnetization loop. One can attain this by tuning the crystalline characteristics of the hard phase to maximize the coupling efficiency.

This work was supported by the ONR/MURI under Grant No. N00014-05-1-0497.

[1] J. S. Jiang, E. E. Fullerton, C. H. Sowers, A. Inomata, S. D. Bader, A. J. Shapiro, R. D. Shull, V. S. Gornakov, and V. I. Nikitenko, IEEE Trans. Magn. **35**, 3229 (1999).
[2] E. E. Fullerton, J. S. Jiang, M. Grimsditch, C. H. Sowers, and S. D. Bader, Phys. Rev. B **58**, 12193 (1998).
[3] H. Fukunaga, N. Kitajima, and Y. Kanai, Mater. Trans., JIM **37**, 864 (1996).
[4] T. Schrefl, J. Fidler, and H. Kronmüller, Phys. Rev. B **49**, 6100 (1994).
[5] R. Skomski and J. M. Coey, Phys. Rev. B **48**, 15812 (1993).
[6] H. Zeng, J. Li, J. P. Liu, Z. L. Wang, and S. H. Sun, Nature (London) **420**, 395 (2002).
[7] G. C. Hadjipanayis, J. Magn. Magn. Mater. **200**, 373 (1999).
[8] J. P. Liu, C. P. Luo, Y. Liu, and D. J. Sellmyer, Appl. Phys. Lett. **72**, 483 (1998).
[9] J. Bauer, M. Seeger, A. Zern, and H. Kronmüller, J. Appl. Phys. **80**, 1667 (1996).
[10] D. Goll, M. Seeger, and H. Kronmüller, J. Magn. Magn. Mater. **185**, 49 (1998).
[11] E. E. Fullerton, J. S. Jiang, and S. D. Bader, J. Magn. Magn. Mater. **200**, 392 (1999).
[12] P. G. McCormick, W. F. Miao, P. A. I. Smith, J. Ding, and R. Street, J. Appl. Phys. **83**, 6256 (1998).
[13] L. Withanawasam, A. S. Murphy, G. C. Hadjipanayis, and R. F. Krause, J. Appl. Phys. **76**, 7065 (1994).
[14] H. Zeng and S. H. Sun, T. S. Vedantam, J. P. Liu, Z. R. Dai, and Z. L. Wang, Appl. Phys. Lett. **80**, 2583 (2002).
[15] J. S. Jiang, J. E. Pearson, Z. Y. Liu, B. Kabius, S. Trasobares, D. J. Miller, S. D. Bader, D. R. Lee, D. Haskel, G. Srajer, and J. P. Liu, J. Appl. Phys. **97**, 10K311 (2005).
[16] D. C. Crew, J. Kim, L. H. Lewis, and K. Barmak, J. Magn. Magn. Mater. **233**, 257 (2001).
[17] H. Zhang, S. Y. Zhang, B. Shen, and H. Kronmüller, J. Magn. Magn. Mater. **260**, 352 (2003).
[18] R. Fischer and T. Schrefl, K. Kronmüller, and J. Fidler, J. Magn. Magn. Mater. **150**, 329 (1995).
[19] E. F. Kneller, and R. Hawig, IEEE Trans. Magn. **27**, 3588 (1991).
[20] H. Kronmüller, R. Fischer, M. Seeger, and A. Zern, J. Phys. D: Appl. Phys. **29**, 2274 (1996).
[21] Y. K. Takahashi, T. O. Seki, K. Hono, T. Shima, and K. Takanashi, J. Appl. Phys. **96**, 475 (2004).
[22] Y. Kubota, L. Folks, and E. E. Marinero, J. Appl. Phys. **84**, 6202 (1998).
[23] Z. H. Cheng, H. Kronmüller, and B. G. Shen, Appl. Phys. Lett. **73**, 1586 (1998).
[24] E. F. Kneller, IEEE Trans. Magn. **27**, 3588 (1991).
[25] E. Goto, N. Hayashi, T. Miyashita, and K. Nakagawa, J. Appl. Phys. **36**, 2951 (1965).
[26] Z. J. Guo, J. S. Jiang, J. E. Pearson, S. D. Bader, and J. P. Liu, Appl. Phys. Lett. **81**, 2029 (2002).
[27] T. Leineweber and H. Kronmüller, J. Magn. Magn. Mater. **176**, 145 (1997).
[28] A. J. Zambano, H. Oguchi, I. Takeuchi, Y. Choi, J. S. Jiang, J. P. Liu, S. E. Lofland, D. Josell, and L. A. Bendersky, Phys. Rev. B **75**, 144429 (2007).
[29] H. W. Xi, B. Bian, K. R. Mountfield, Z. L. Zhuang, D. E. Laughlin, and R. M. White, J. Magn. Magn. Mater. **260**, 273 (2003).
[30] E. E. Fullerton, J. S. Jiang, C. H. Soweres, J. E. Pearson, and S. D. Bader, Appl. Phys. Lett. **72**, 380 (1998).
[31] J. Kim, K. Barmak, M. De Graef, L. H. Lewis, and D. C. Crew, J. Appl. Phys. **87**, 6140 (2000).
[32] M. Yu, J. Hattrick-Simpers, I. Takeuchi, J. Li, Z. L. Wang, J. P. Liu, S. E.

Loftland, S. Tyagi, J. W. Freeland, D. Giubertoni, M. Bersani, and M. Anderle, J. Appl. Phys. **98**, 063908 (2005).
[33]M. Murakami, S. Fujino, S.-H. Lim, L. G. Salamanca-Riba, M. Wutting, I. Takeuchi, B. Varughese, H. Sugaya, T. Hasegawa, and S. E. Lofland, Appl. Phys. Lett. **88**, 112505 (2006).
[34]M. Abes, O. Ersen, C. Meny, G. Schmerber, M. Acosta, J. Arabski, C. Ulhaq-Bouillet, A. Dinia, P. Panissod, and V. Pierron-Bohnes, J. Appl. Phys. **101**, 063911 (2007).
[35]M. Yu, H. Oguchi, A. J. Zambano, I. Takeuchi, J. P. Liu, D. Josell, and L. A. Bendersky, Mater. Sci. Eng., B **142**, 139 (2007).
[36]JCPDF Card No. 43–1358.
[37]Y. Suzuki, R. B. vanDover, E. M. Gyorgy, J. M. Phillips, and R. J. Felder, Phys. Rev. B **53**, 14016 (1996).
[38]Y. Suzuki, Annu. Rev. Mater. Res. **31**, 265 (2001).